Eigenfrequencies of rotating discs in dense fluid: imposed modal motion approach

Eigenfrequencies of rotating discs in dense fluid: imposed modal motion approach

B Nennemann[1], C Monette[1], O Braun[2], Daniel Biner[3], Cécile Münch-Alligné[3]

[1]Andritz Hydro Canada Inc., Montreal, Canada
[2]Andritz AG, Graz, Austria
[3]HES-SO Valais, Switzerland

bernd.nennemann@andritz.com

Abstract. The mode split on disc like structures rotating in a dense fluid leads to a deviation of eigenfrequencies at high rotational speeds compared to their values in still water. Predicting eigenfrequencies correctly is essential to avoid fatigue cracks on prototype turbine runners. Analytical models for simple geometric configurations and complex numerical models using fully coupled fluid structure interaction to predict the mode split on arbitrary geometries exist. We are presenting a complementary approach of intermediate complexity applicable to arbitrary geometries. Mode shapes and modal parameters are computed by finite element analysis in still water. These mode shapes are imposed with a harmonic variation in time during an unsteady computational fluid dynamics computation. From the interaction between the flow and the modal motion, the modal force and the modal work can be computed. These can be converted into added modal mass and hydrodynamic damping and further into the shift of the eigenfrequency under rotation due to the fluid for a given mode. The tendencies of the frequencies with rotation compare reasonably well with experimental data. The numerical method can be applied to disc rotation speeds far beyond the range of experimental data revealing interesting tendencies and a phenomenological interpretation of the cause of the mode split.

1. Introduction

Crown and band of high head turbines and pump turbines resemble rotating discs, especially on the sides facing the respective crown and band chambers. A typical shape of a pump turbine runner is shown, in Figure 1 (a) (adopted from [1]). Typical mode shapes on such structures consist of nodal diameters k and nodal circles s, 3 and 0 shown respectively in Figure 1 (b). They are composed of co- and counter-rotating waves with respect to the fluid rotation relative to the disc, see Figure 1 (c). If a disc rotates in a dense fluid, the co- and counter-rotating wave frequencies evolve differently. The split between the two increases with speed, while the average value decreases as illustrated in Figure 1 (d). With respect to hydraulic pumps, the effect of rotation on the eigenfrequencies and stability of circular discs has first been recognized by Kubota et al. [2]. Early experimental and analytical work on this topic in the hydraulic turbine literature was published by Presas et al. [3]-[5] and Valentin [6], and a numerical study using fully coupled fluid structure interaction (FSI) by Weber et al. [7]. Louyot et al. [1] generalized the analytical model for a rotating disc in water within a rigid casing. Their analytical approach was extended by Berthet [8] to account for radial wall proximity and stator disc flexibility. Detailed experimental results on the mode split phenomenon with a flexible rotor and stator are presented by Weder [9].

Experimental results on the phenomenon of the rotating disc mode split such as [3] and [9] are fundamental to explore the underlying physics and to provide data for the validation of analytical and numerical models. Analytical solutions to the disc mode split phenomenon are useful in identifying the basic physics and the main parameters of influence ([1], [4]). Once validated, they can be used to explore ranges of the geometric and physical parameters that are difficult to attain in measurements ([1]). While numerical approaches such as the full two-way fluid structure interaction in [7] are applicable to arbitrarily complex geometries, they are also time and resource intensive. The modal finite element analysis (FEA) and computational fluid dynamics (CFD) based approach we are presenting here is of intermediate complexity and computational resource intensity, yet it can also be applied for arbitrary geometries such as hydraulic turbine runners.

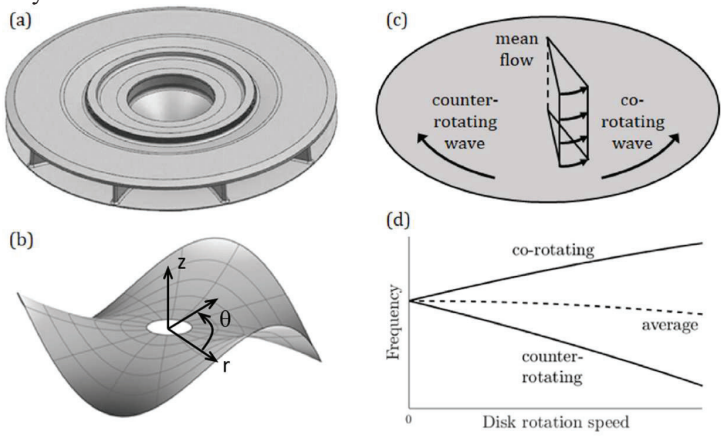

Figure 1. (a) A pump-turbine runner geometry. (b) A typical disc mode shape with 3 nodal diameters and 0 nodal circles. (c) Each disc mode is composed of a co-rotating and a counter-rotating wave with respect to the fluid rotation relative to the disk. (d) Co- and counter-rotating wave frequencies vary with the disc rotation speed in dense fluid (adopted from [1])

The purpose of predicting the mode split on turbine runners is an accurate prediction of all relevant eigenfrequencies. This is of high importance for high head turbines and pump turbines since these tend to have strong rotor stator interaction (RSI) between the guide vanes and the runner blades, e.g., [10]. Predicting the potential presence of resonance during the design phase is therefore essential to avoid the risk of fatigue cracks on the prototype runner.

2. Vibration modes of circular discs

On circular discs such as the one shown in Figure 1 (c), made up out of a homogenous elastic material, a disturbance resulting in a vibration, a hit with a hammer for example, will propagate as waves. In the circumferential direction, wave propagation has no preferred direction and will therefore propagate "forward" and "backward" or as expressed alternatively as "co-" and "counter-rotating" waves relative to the fluid rotation shown in Figure 1 (c). We use + and – as notation for "forward" and "backward". For eigenmodes, to satisfy circular periodicity, these waves must consist of an integer multiple (including zero) of a full sine wave. The number of sine waves defines the number of nodal diameters k. In the radial direction, eigenmodes will have integer numbers of radial circles s with no displacement. From the representation of a basic harmonic wave $w(\theta,t) = \hat{w}\,cos(k\theta - \omega t)$, the displacements from the superposition of a pair of forward and backward waves can be expressed as

$$\begin{aligned} w(r,\theta,t) &= w(r)[cos(k\theta - \omega_+ t) + cos(k\theta + \omega_- t)] \\ &= w(r)[cos(k\theta)\,(cos(\omega_+ t) + cos(\omega_- t)) + sin(k\theta)\,(sin(\omega_+ t) - sin(\omega_- t))] \\ &= w_{c.n}(r,\theta)u_c(t) + w_{s.n}(r,\theta)u_s(t) \end{aligned} \quad (1)$$

according to [1] where w is the displacement in the z-direction, $\omega_{+/-}$ are the angular frequencies and t is the time. The second line is obtained by using trigonometric identities and represents a decomposition

into a cosine and a sine component of the mode of vibration as well as a separation of the spatial and temporal components. The cosine and sine mode shapes $w_{c.n}$ and $w_{s.n}$ are referred to as companion modes in [1], and can also be interpreted as the real and imaginary parts of a complex mode, which we normalize to a max displacement of 1 here. If assumed constant, the angular phase velocities (denoted by ω_φ) for the forward and backward waves are obtained by setting the time-derivatives of the arguments of the cosine functions in the first line of equation (1) to zero and are as stated in [11]

$$\omega_{\varphi+} = \frac{d\theta}{dt} = \frac{\omega_+}{k}, \omega_{\varphi-} = \frac{\omega_-}{k} \tag{2}$$

Since angular frequencies $\omega_{+/-}$ are, by definition, positive, the sign of the angular phase velocities ω_φ is obtained through a positive or negative sign of the nodal diameter number k. On circular discs at standstill, eigenmode vibrations at resonance will be observed as standing waves since they are a superposition of the forward and backward waves, which both have the same angular phase velocity magnitude but opposite directions. As mentioned in the introduction, vibration eigenmodes and frequencies of circular discs in a still fluid can be calculated analytically [1] or by means of acoustic finite element modal analysis.

3. Mode split phenomenon

Weder et al. [9] investigated a configuration of two flexible circular discs experimentally of which one (rotor) is fully submerged in water and can be rotated in proximity of a circular, thin casing wall (stator). A schematic representation of their setup is shown in Figure 2 (a). Excitation is performed per frequency sweep at a point-location on the stator. In the example of a measurement result in Figure 2 (b) for a single vibration amplitude peak at zero rotation, two corresponding vibration peaks occur at a rotation speed of $\Omega_R = 50.3\ rad/s$. This is the mode split phenomenon.

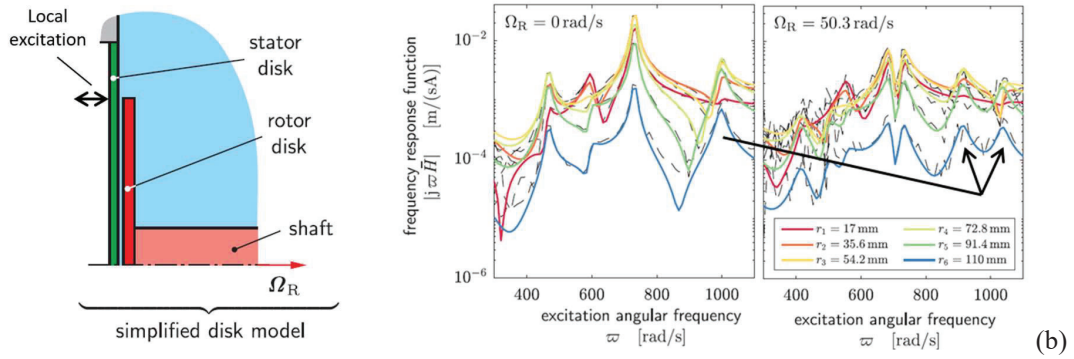

Figure 2. (a) Schematic rotor-stator disc configuration and (b) frequency sweep results with and without rotation measured on the stator disc, adopted from [9]

In [1] the effective fluid angular velocity Ω_F is related to the disc rotation Ω_R by an entrainment coefficient $K_{\alpha.F}$

$$\Omega_{F,r} = K_{\alpha.F}\Omega_R, \qquad \Omega_{F,s} = (1 - K_{\alpha.F})\Omega_R \tag{3}$$

Upper case subscripts F, S, R indicate "of which component" while lower case subscripts f, s, r, indicate "observed from which component", e.g., $\Omega_{F,r}$ is the angular velocity of the fluid seen from the rotor. According to the literature, the entrainment coefficient is typically $K_{\alpha,F} = 0.5 \ldots 0.6$.

The data from [9] in Figure 3 show that on the stator the eigenfrequency of the forward wave increases with rotation speed while it decreases for the backward wave. On the rotor it is the other way around. The frequency split is smaller on the stator than on the rotor because the flow entrainment is less as observed from the stator than from the rotor ($(1 - K_\alpha)$ vs K_α, distinct from $K_{\alpha,F}$ as will be explained in the discussion). Part (a) of the figure illustrates that there is a frequency drift in addition to

a frequency split. In Figure 3 (b) the differences between the forward and the backward waves on the rotor and the stator are practically linear as a function of rotor speed. The light-grey short-dashed lines show the difference of the frequencies of a single wave (i.e., forward or backward) as seen from the rotor and the stator, confirming that the kinematic transformation $k\Omega_R$ from one frame to the other is almost exactly measured.

Assuming the change in added mass of the fluid with rotation is the dominant driving mechanism in the frequency split, the change and split of frequencies can be explained by the change of fluid inertial reaction between flowing with the waveform versus against the waveform, leading to an apparent shorter, respectively longer waveform for an entrained fluid particle. The dependency of wavelength on the used reference frame is shown in Figure 4.

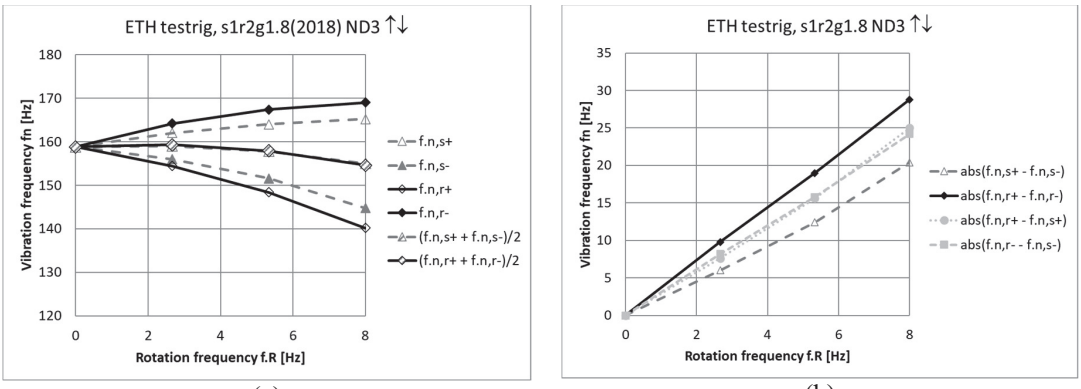

(a) (b)

Figure 3. (a) Measured eigenfrequencies on stator and rotor for forward and backward waves as a function of disc rotation frequency (b) difference of eigenfrequencies from forward and backward waves on rotor and stator, i.e., frequency split; (a) and (b) with data from [9] for a 3 nodal diameter counter-phase mode

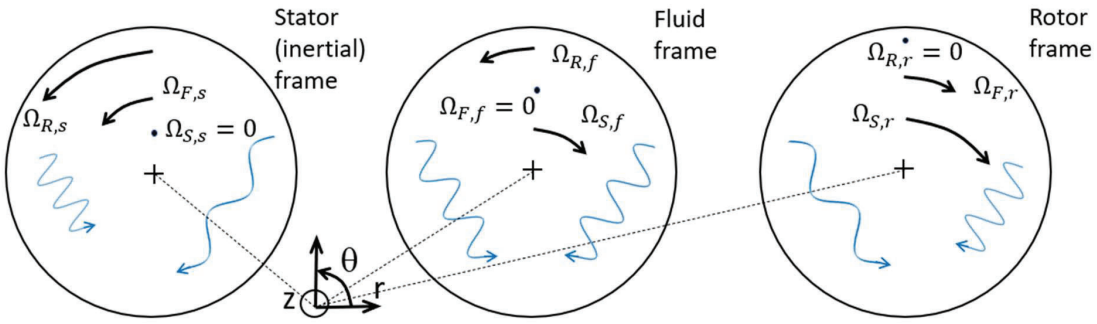

Figure 4. Schematic wavelength stretching and compression depending on the reference frame. In the fluid reference frame, forward and backward waves have the same wave propagation properties.

Previous, fluid-centric studies [1], [2] suggest considering a frame rotating with the average fluid velocity, so that the fluid behaviour in this frame is equivalent to the standstill situation and independent of the direction of the wave. Such considerations create a direct link of the shift of eigenfrequencies to the rotation velocity of the fluid flow, such that the asymmetry of the split can be explained. In this fluid-centric interpretation of the mode split, for a given mode with k nodal diameters, an angular

eigenfrequency ω_n and an effective fluid angular velocity Ω_F, there would be a single wave propagation angular velocity magnitude for the forward and the backward wave:

$$\omega_{\varphi n,f} = \frac{\omega_{n,f}}{k} \tag{4}$$

The angular frequency of a time-varying displacement at a location seen from the stator or rotor reference frame for a forward or backward wave would then be observed as

$$\omega_{n,xy} = k(\omega_{\varphi n,fy} + \Omega_{F,x}) \tag{5}$$

where $x = r$ or s indicate, if it is from the rotor or the stator, and $y = +$ or $-$, if it is for a forward or backward wave. The sign of the nodal diameter number k determines the direction of a wave, positive for a forward and negative for a backward wave. The water angular velocity $\Omega_{F,x}$ is positive in the stator frame and negative in the rotor frame for a positive rotor angular velocity Ω_R. The mode split is reflected in the signs of k and $\Omega_{F,x}$. Both waves have the same fundamental properties of wave propagation with the same magnitude of $\omega_{\varphi n,f}$, but the eigenfrequencies and consequently the frequencies to excite them as vibration modes differ from the forward to the backward waves. Note again, that these are structural or flexural rather than acoustic waves.

The frequency drift cannot be explained in as simple a manner as the frequency split. However, it is the same for forward and backward waves. This was also shown by Louyot's [1] analytical model.

The imposed modal motion approach presented in this paper avoids the complexity of working with shifting frames, by simply identifying the fluid's integrated answer to an imposed mode shape vibration under different flow conditions.

4. Numerical modelling

4.1. Finite element modal analysis

The numerical approach we present here is mode based. The computation of the actual added modal mass to account for the mode split is done in CFD. In CFD a modal motion is imposed in the form of time varying mesh displacement. Mode shape and other modal parameters such as modal mass and modal stiffness can be calculated analytically for simple geometries [1] or numerically by means of finite element modal analysis. This can be done for the structure in still water using acoustic elements to capture the effect of the presence of the fluid. The approach is standard in the hydraulic turbine industry. The specifics of the modal analysis used for this study can be found in [11]. Knowing that for the investigated case, the modal mass of the fluid is above 90% of the total modal mass, and that eigenfrequencies of the structural parts in air are four to five times higher than the coupled system frequency, we assume that these mode shapes remain unchanged in the rotating, vibrating system. This may be a good approximation, but its range of validity should be investigated in detail in the future.

4.2. Computational Fluid Dynamics setup

The imposed modal motion approach, sometimes referred to as modal work approach, has been used to calculate hydrodynamic damping, e.g., [13]-[14]. It can also be used to calculate the water added modal parameters, i.e., the water added mass and stiffness. Biner [11] investigated the imposed modal motion approach to predict the frequency split on the same configuration as presented here. At the time of that study, it was not clear how to extract the frequency split from the CFD results.

An alternative modal approach is the coupling of two single degree of freedom (1dof) oscillator models to represent the two companion modes $u_c(t)$ and $u_s(t)$ from equation (1) within the CFD model. Free oscillations of wave modes are then possible and the eigenfrequencies can be extracted from the results. This approach was used by Louyot et al. [1]. It is conceptually attractive but proved to be a numerical challenge. Imposed modal motion approaches tend to be numerically more robust.

Figure 5 shows the mesh we used as well as a contour plot of the mesh displacement on the rotor and the stator for a 3 nodal diameter ($k = 3$) counterphase mode shape. The mesh contains about 410k nodes. We used the commercial CFD code Ansys CFX version 2019R1 with the $k - \varepsilon$ turbulence model and CFX's high resolution scheme for advection and turbulence. The transient calculation was performed

with 200 time steps per period of mesh motion and three coefficient loops most of the time. For an accurate damping prediction, the maximum residuals must be below 1e-6, and therefore more coefficient loops are needed. This simple approach (coarse mesh and standard turbulence model) was considered justified because the frequency split phenomenon appeared to be primarily a potential effect based on the fact that it can be predicted analytically using a potential flow solution [1], [8]. The main effect of viscosity is on the entrainment coefficient $K_{\alpha,F}$, which is an input to analytical models. Since we use single phase incompressible CFD, acoustic effects are not captured. So, any wave propagation we refer to here is the propagation of structural wave modes with the structure in water, rather than a propagation of acoustic waves in water.

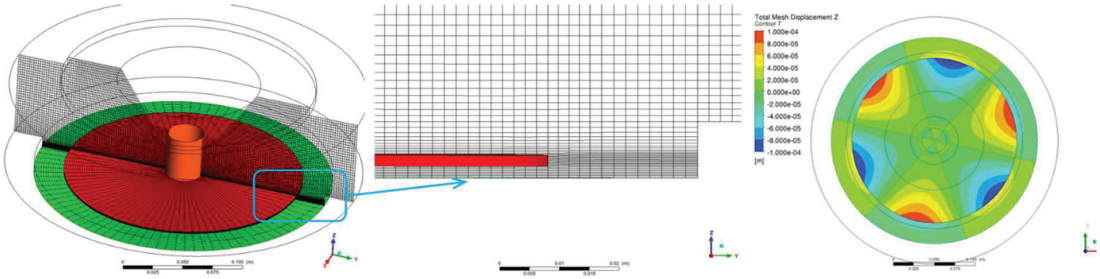

Figure 5. Basic mesh for CFD calculations of rotor stator configuration (as shown in **Figure 2** (a)) with 410k mesh nodes and a 3 nodal diameter out-of-phase mode imposed on the rotor and stator surface meshes.

4.3. Extraction of added modal parameters

In general, we impose either a forward or a backward wave according to equation (1) in the CFD calculations where $w_{c.n}(r,\theta)$ and $w_{s.n}(r,\theta)$ are normalized mode shapes with a maximum reference displacement of 1. The time-dependent terms in equation (1) ($u_c(t)$ and $u_s(t)$) are set to a suitable physical reference amplitude, $\hat{u}_{ref} = 0.1\ mm$ for example. This is done in the rotating or stationary frame of reference. Figure 6 (a) shows the behavior of two monitor points, one rotated by 30° relative to the other, at the same radius on each of the stator and the rotor. The curves illustrate the phase shift in time between points on either the rotor or the stator, and the "out-of-phase"-ness of the rotor with the stator. In this example a backward wave is shown.

A modal force within a CFD calculation is calculated with a surface integral of the scalar product between the wall pressure p and shear $\underline{\tau}$ components and the normalized mode shape $\underline{w}(r,\theta) = \left(\underline{w}_{c.n}(r,\theta) + \underline{w}_{s.n}(r,\theta)\right)$

$$F_m = \int_A (p\underline{n} + \underline{\tau}) \cdot \underline{w}(r,\theta) dA \tag{6}$$

where underscores indicate vectors. This is a function of time because pressure and shear are functions of time. (We added the underscore to the normalized mode shape here for the sake of generality. In equation (1) this was omitted since the dominant displacement is in the z-direction only).

Since the 1dof oscillator equations of motion apply to a mode, its dynamic behaviour, in our case with the presence of water, can be described by

$$F_m(t) = (M_s + M_w + M_f)\ddot{u}_r + (B_s + B_w + B_f)\dot{u}_r + (K_s + K_w + K_f)u_r \tag{7}$$

with the reference displacement u_r, the modal mass M, the modal damping coefficient B and the modal stiffness K, and the subscripts s for structure, w for still water and f for flow. Structural damping does not need to be considered for our analyses. Finite element analysis with acoustic elements will deliver $M_s + M_w \equiv M_{sw}$ and $K_s + K_w \equiv K_{sw}$. In CFD with the imposed modal motion, the water and flow contributions of the modal mass and damping as well as the flow added stiffness are included in the modal force

$$F_{m.CFD}(t) = M_{wf}\ddot{u}_r + B_{wf}\dot{u}_r + K_f u_r \tag{8}$$

Using the particular solution of the differential equation for a forced harmonic oscillator $u_r(t) = \hat{u}_r \cos(\omega_e t - \varphi)$ where $\hat{u}_r$ is the oscillation reference amplitude, ω_e the excitation angular frequency and φ the phase between the forcing and the response, we obtain for the force amplitude (dropping CFD from the subscript)

$$\hat{F}_m = \sqrt{\left(K_f \hat{u}_r - M_{wf}\hat{u}_r\omega_e^2\right)^2 + \left(B_{wf}\hat{u}_r\omega_e\right)^2} \tag{9}$$

Since we are only interested in the change in eigenfrequency due to rotation, we can drop $K_f\hat{u}_r$ for simplicity. Its contribution is then accounted for by the modal mass which we call $M_{wf,K}$. In [13] it is shown how K_f can be accounted for separately. The water and flow added damping can be calculated from the modal work per period of oscillation as shown in [13] and [14] by

$$B_{wf} = -W_{m.T}/(\pi\omega_e\hat{u}_r^2) \tag{10}$$

The modal work per period of oscillation is computed from CFD by

$$W_{m.T} = \int_{t=0}^{T}\int_{A}(p\underline{n} + \underline{\tau})\cdot\dot{u}_r\underline{w}(r,\theta)dA\,dt \tag{11}$$

where the time derivative of the modal motion is equal to the mesh velocity in CFD.

In summary, using $W_{m.T}$ from CFD to calculate B_{wf} we can use $\hat{F}_m$ from CFD and equation (9) to calculate the water and flow added modal mass including the contribution of flow added stiffness $M_{wf,K}$. Then the angular eigenfrequency of the combined rotor and stator disc coupled by the fluid under rotation can be calculated from

$$\omega_n^2 = K_{sw}/(M_s + M_{wf,K}) \tag{12}$$

with the modal stiffness of the structure M_s and the stiffness of the structure in still water K_{sw} from finite element modal analysis.

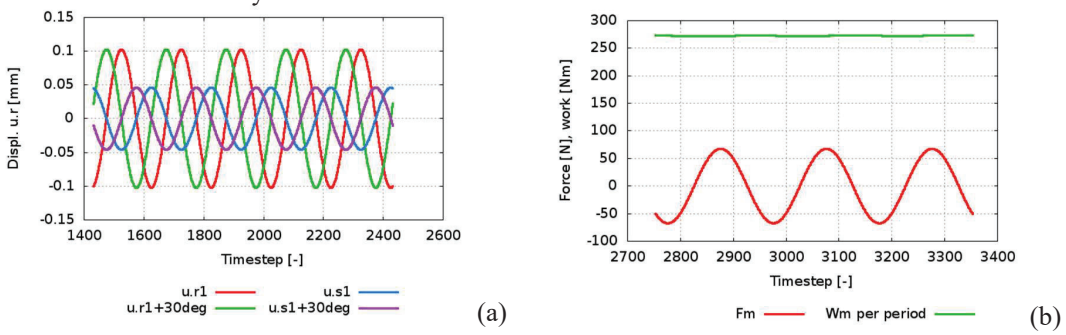

Figure 6. From CFD: (a) displacements at two monitor points on each rotor and stator of a counter-rotating wave of a 3 nodal diameter out-of-phase mode (b) modal force and modal work per period of oscillation of the same computation.

5. Results and Discussion

The eigenfrequencies calculated with the imposed modal motion approach shown in Figure 7 (a) have similar tendencies as the experimental results shown in Figure 3 (a): the frequency on the stator increases with the forward (+) and decreases with the backward (-) wave, and on the rotor it is the other way around. The frequency split is smaller on the stator than on the rotor. There is an offset at zero rotation of around 4%, because the modal mass and stiffness parameters do not result in the same eigenfrequency in still water as the experiments. We used the modal parameters from the analytical solution by Berthet [8]. The predicted frequency split is smaller than the measured one by about 18% as is clear from Figure 7 (b). This is reasonable. Improvements may be possible with a refined CFD approach. Here, experimental data are only given for the stator reference frame. The relatively strong frequency drift that is seen in the measurements is absent from the predictions. At this point, the cause for the absence of

the frequency drift is not clear. Since it is small for low rotational speeds, the frequency drift is less significant than the frequency split from a practical point of view regarding hydraulic turbines.

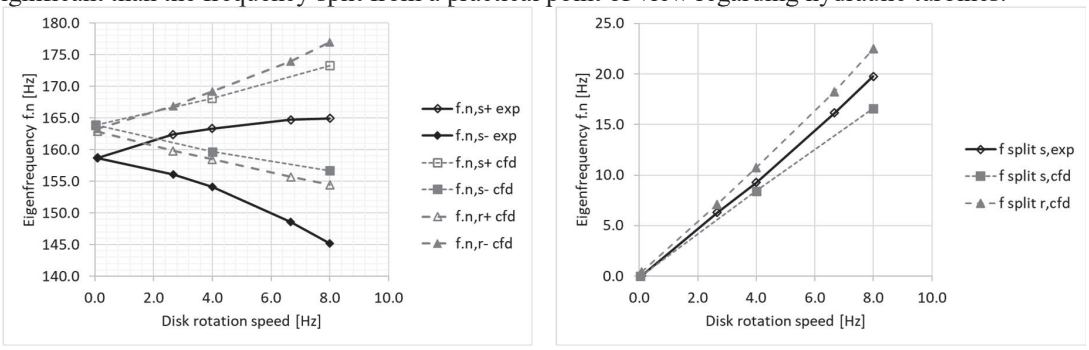

(a) (b)

Figure 7. Comparison of measured and CFD-calculated eigenfrequencies in (a) and frequency split between forward and backward waves in (b) as a function of disc rotation frequency for a 3 nodal diameter counter-phase mode, experimental data from [9].

If the frequency split has been measured or calculated for a given rotation speed, by using equation (5) the entrainment coefficient can be calculated for the forward and backward waves:

$$K_\alpha = \frac{1}{2\Omega_R}\left(\frac{\omega_{n,r+}}{k_+} + \frac{\omega_{n,r-}}{k_-}\right), K_\alpha = 1 - \frac{1}{2\Omega_R}\left(\frac{\omega_{n,s+}}{k_+} + \frac{\omega_{n,s-}}{k_-}\right) \quad (13)$$

This entrainment can be considered as an expression of the mode split and represents the coupling of the structural wave mode or modes (rotor and stator) and the fluid, and we distinguish it from the pure fluid flow entrainment $K_{\alpha,F}$. The entrainment coefficients calculated from the measurements and our CFD simulations are summarized in Table 1. For the experimental results the values from the rotating and stationary frames of reference are consistent. Since the frequency split is not predicted exactly by CFD as shown above, the corresponding entrainment coefficients do not match the experimental ones. Furthermore, the entrainment coefficients from CFD in the rotating frame are not consistent with those from the stationary frame as they do not sum to 1. Both these aspects indicate that the accuracy of CFD to predict the mode split should be improved. Our initial assumption that a simple CFD approach should be sufficient because analytical approaches can capture the mode split is therefore not confirmed. The effects of changing solid behaviour under rotation may need to be taken into account to achieve more accurate results, which excludes using the presented approach of imposing a fixed mode shape to determine modal forces, thus fluid modal properties at various rotation rates as the main driver of the mode split. The results also imply that the entrainment coefficient is a key parameter for the accuracy of analytical models. In this sense the entrainment coefficient K_α is a mental model and is different from the pure fluid entrainment coefficient $K_{\alpha.F}$. For comparison, the entrainment coefficient $K_{\alpha.F}$ based on the average flow velocity from CFD in the gap between the rotor and the stator, and as used by Louyot [1], is given in the Table 1 (6th column).

Table 1. Entrainment coefficients

		Exp.	CFD		From ave. flow vel. CFD
Rot. ref. frame	$\boldsymbol{K_\alpha}$**:**	0.60	0.45	$\boldsymbol{K_{\alpha,F}}$**:**	0.55
Stat. ref. frame	$\boldsymbol{1-K_\alpha}$**:**	0.40	0.65	$\boldsymbol{1-K_{\alpha,F}}$**:**	0.46

In Figure 8 the relative eigenfrequency f_n/f_{n0}, i.e., the ratio of the eigenfrequency f_n over the eigenfrequency in vacuum f_{n0}, is plotted over the normalized relative angular phase velocity $\varphi_{rel.n}$. The latter is the angular phase velocity of the wave ω_e/k, imposed or measured, minus the angular effective flow velocity Ω_F normalized with the angular phase velocity:

$$\varphi_{rel.n} = (\omega_e/k - \Omega_F)/(\omega_e/k) \quad (14)$$

Figure 8 (a) shows the range for which measurement results exist. The measurement data from Figure 7 (a) (black line, diamonds) form a single line for the forward and backward wave. By definition $\varphi_{rel.n} = 1$ separates the forward and backward waves. The same is the case for the CFD results (grey lines: squares and triangles). They form relatively straight continuous lines for the sections corresponding to the forward and backward waves. In addition, the results calculated in the rotating and stationary reference frames fall practically one on top of the other. The main offset between the experimental and CFD results in this representation is due to the difference in eigenfrequency in still water, i.e., at zero rotation as mentioned above.

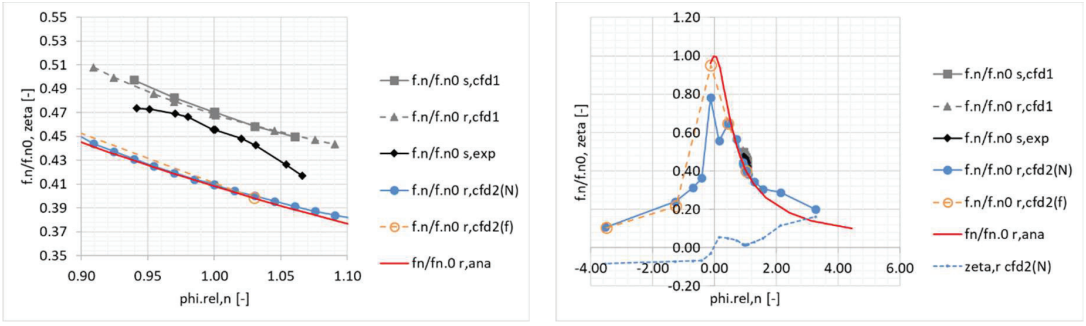

(a) (b)

Figure 8. Representation of experimental, CFD and analytical results in the form of relative eigenfrequency over relative phase velocity with $K_\alpha = 0.60$. Results become independent of reference frame and type of calculation, i.e., by variation of disc rotation speed (N) or forcing frequency (f). (a) shows the range covered by experiments and (b) the full range that has been calculated by CFD.

A second set of CFD results (cfd2) with a different gap between rotor and stator is slightly off-set compared to our main validation results. For this configuration a large range of imposed frequencies (f) and rotational speeds (N) was calculated. Results are presented to illustrate the tendencies that arise from such a parameter variation. In addition, equation (61) from Louyot et al. [1], referred as "ana", is plotted for this second gap configuration:

$$\omega_n = \left(\sqrt{(\beta_0 + 1)\omega_{n0}^2 - \beta_0\left(k\Omega_{F,r}\right)^2} - k\beta_0\Omega_{F,r}\right)/(\beta_0 + 1) \quad (15)$$

Parameter β_0 in that equation, representing geometrical and material properties, is adjusted to 5 such that the value of the equation matches the "cfd2" curve at $\varphi_{rel.n} = 1$ as can be seen in Figure 8 (a).

Plotting f_n/f_{n0} over $\varphi_{rel.n}$ in Figure 8 (b) over a much larger range leads to a unified representation of the mode split results. Eigenfrequencies calculated (or measured) in the rotating or stationary frame of reference as well as those calculated either by variation of the rotor speed ($0 \ldots 24000\ rpm$) or by variation of the forcing frequency ($20 \ldots 3000\ Hz$) fall onto normalized curves that are relatively close to each other. The largest deviations between different CFD calculations occur around $\varphi_{rel.n} = 0$ where the modal force amplitude approaches zero and the flow becomes numerically challenging.

As a general tendency, the relative eigenfrequency increases with a decreasing difference between the flow velocity and the wave propagation speed. As zero is approached, f_n/f_{n0} approaches 1. This was also noted by [2] and can be interpreted as the water no longer providing any inertial reaction to the vibration, and the frequency therefore approaching its value in vacuum. The damping ratio ζ calculated from the modal work per period of oscillation is positive over all positive values of $\varphi_{rel.n}$ but has a local minimum near 1 where the wave direction changes from backward to forward (with increasing $\varphi_{rel.n}$). For $\varphi_{rel.n} < 0$ the frequency decreases again. Damping becomes negative indicating self-excitation. The analytical curve matches the CFD curve reasonably well, indicating that the analytical solution and CFD represent the same basic physics. The experimental entrainment coefficient of $K_\alpha = 0.60$ is used.

6. Summary and conclusion

Our study presents a combined FEA and CFD based modal approach, showing how the fluid added mass part of the mode split can be computed numerically. A conversion of modal force and modal work into an added modal mass and therefore shift of eigenfrequency under rotation is given. It assumes that the dynamic behaviour of a mode follows the behaviour of a single degree of freedom oscillator and that the mode shape and structural modal parameters on rotor and stator are unchanged from their form and values at standstill. The validity of these assumptions may require scrutiny in the future. While the tendencies of the eigenfrequencies with rotation are correctly captured, the frequency split magnitude is underpredicted. In terms of practical application of the method in the design of hydraulic machines, future improvements are desirable. However, being able to consider the mode split with this inaccuracy is already a significant improvement over not being able to account for it at all.

Plotting the normalized eigenfrequencies over the normalized difference between the structural angular wave propagation velocity and the fluid angular velocity results in a relatively unified curve for all parameter combinations. This implies that the difference between the angular wave propagation velocity and the fluid angular velocity plays a significant role in the physics of the mode split on discs rotating in a dense fluid. Clearly, there are still many open questions to be addressed in the future.

Acknowledgments

Special thanks to Max Louyot and Lucas Berthet for their excellent analytical work in their MSc projects.

References

[1] Louyot M Nennemann B Monette C Gosselin F P 2020 Modal analysis of a spinning disk in a dense fluid as a model for high head hydraulic turbines, *J. of Fluids Struct* **94**
[2] Kubota Y Ohashi H 1991 A study on the natural frequencies of hydraulic pumps *Proc. 1st ASME Joint Int. Conf. Nuclear Eng* Tokyo Japan pp. 4–7.
[3] Presas A 2014 *IOP Conf. Ser.: Earth Environ. Sci.* **22** 032043
[4] Presas A 2015 *J. Sound Vib.* **337**, 161–180
[5] Presas A Valentín D Egusquiza E Valero C Seidel U 2016 Dynamic response of a rotating disk submerged and confined, Influence of the axial gap. *J. of Fluids Struct* 62, 332–349.
[6] Valentín D Presas A Egusquiza E Valero C 2014 Exp study on the added mass and damping of a disk submerged in … *J of Fluids Struct*. **50**, 1–17
[7] Weber W Seidel U 2015 Analysis of natural freq of disc-like structures in water env by coupled fluid–structure-interaction sim *6th IAHR WG on Cav Dyn Probs in Hyd Mach Sys*
[8] Berthet L 2021 Mode Split Prediction for Rotating Disks with Flexible Stator Coupling MSc Thesis École Polytechnique de Montréal
[9] Weder M Horisberger B Monette C Sick M Dual J 2019 Experimental modal analysis of disk-like rotor–stator system coupled by viscous liquid *J. Fluids Struct.* **88** 198–215
[10] Coutu A et al 2008 Experience with Rotor-Stator interactions in high head Francis runner *24th Symposium on Hydraulic Machinery and Systems* Foz do Iguazu Brazil
[11] Biner D 2017 Hydrodynamic Damping and Added Stiffness Prediction on a Rotor-Stator Disk Assembly in Water using a Modal Approach MSc HES-SO
[12] Münch C, Ausoni P, Braun O, Farhat M and Avellan F 2010 Fluid-structure coupling for oscillating hydrofoil *J. of Fluids Struct* **26** 1018-33
[13] Nennemann B Monette C Chamberland-Lauzon J 2016 Hydrodynamic damping and stiffness prediction in Francis turbine runners using CFD *IOP Conf. Ser.: Earth Environ. Sci.* 49
[14] Gauthier JP Giroux AM Etienne S Gosselin FP 2017 A numerical method for the determination of flow-induced damping in hydroelectric turbines *J. of Fluids Struct* **69** 341-354